Robust networks of interfacial localized graphene in cocontinuous polymer blends

Yangming Kou, Aaron T. Cote, Jiayang Liu, et al.

Citation: Journal of Rheology **65**, 1139 (2021); doi: 10.1122/8.0000294
View online: https://doi.org/10.1122/8.0000294
View Table of Contents: https://sor.scitation.org/toc/jor/65/6
Published by the The Society of Rheology

Robust networks of interfacial localized graphene in cocontinuous polymer blends

Yangming Kou, Aaron T. Cote, Jiayang Liu, Xiang Cheng,[a] and Christopher W. Macosko[a]

Department of Chemical Engineering and Materials Science, University of Minnesota, 421 Washington Avenue SE, Minneapolis, Minnesota 55455

(Received 20 April 2021; final revision received 2 August 2021; published 7 September 2021)

Abstract

Conductive polymer composites enjoy specialized applications such as electrostatic discharge protection. In this work, we create interfacially localized graphene nanoplatelets (GNPs) in a cocontinuous polymer blend of polylactide (PLA) and poly(ethylene-*co*-vinyl acetate) (EVA). Based on the wetting coefficient analysis, GNPs favor localization in the EVA phase. A two-step compounding sequence is designed such that a PLA/GNP masterbatch is first prepared via solution blending, and then melt compounded with the EVA. In the second step, GNPs transfer from the PLA phase to the EVA phase but become kinetically trapped at the interface, as confirmed by electron microscopy. We achieve an ultralow percolation threshold of 0.048 wt. % GNPs and obtain blends with electrical conductivities of $\sim 10^{-5}$ S/cm at 0.5 wt. % GNP concentration. We systematically study the shear and extensional rheology of the ternary composite system. Cocontinuous blends with interfacial GNPs exhibit higher shear and extensional viscosities compared to samples with GNPs localized entirely within the EVA phase. Rheology, *in situ* dielectric measurements, and transmission electron microscopic imaging after nonlinear deformations all show the interfacial GNP network undergoes structure recovery and largely remains at the PLA/EVA interface. Moreover, high electrical conductivity is maintained during 2–10 min melt compounding and conductivity recovers with annealing after nonlinear deformations. These results suggest that these robust GNP networks preserve their bulk electrical conductivity during subsequent melt processing. https://doi.org/10.1122/8.0000294

I. INTRODUCTION

Polymer/graphene systems are potentially advantageous for creating electrically conductive composites for industrial applications such as electrostatic discharge protection and electromagnetic interference shielding. Graphene nanoplatelets (GNPs) are two-dimensional nanomaterials consisting of a few layers of stacked graphene sheets. GNPs exhibit superior material properties such as mechanical strength and high thermal conductivity. Their inherently high electrical conductivity and aspect ratio allow the formation of well percolated filler particle networks when loaded in a polymer matrix. The feature allows dramatic reduction in particle loading and improved melt processability in the production of electrically conductive polymer composites as compared to using traditional fillers such as carbon black (CB) [1].

One main challenge that limits the use of GNPs to construct conductive composites is their relatively high cost compared to CB. To address this challenge, many recent works have focused on controlling particle localization to achieve enhancement in electrical conductivity with minimal filler concentration. Mao *et al.* showed that blending octadecylamine-functionalized graphene nanosheets into a cocontinuous blend of polystyrene (PS)/poly (methyl methacrylate) (PMMA) in which graphene selectively locates and percolates in the PS phase reduces the conductive percolation threshold to 0.5 wt. %, compared to 2 wt. % for similarly prepared homopolymer/graphene composites [2]. The localization of fillers in a cocontinuous polymer blend is determined by the surface energies of the fillers and the two polymer components. When fillers are melt compounded with most polymer pairs, they will selectively localize either within a preferred polymer phase or at the interface to minimize the overall system free energy. Similarly, many previous studies have demonstrated that selective GNP localization within one of the two cocontinuous polymer phases can result in a 2–4-fold decrease in the percolation threshold using both immiscible blends [e.g., PS/polylactide (PLA) [3], polycarbonate (PC)/poly(styrene-*co*-acrylonitrile) (SAN) [4]] and miscible blends [e.g., PMMA/SAN [5], PMMA/poly(α-methylstyrene-*co*-acrylonitrile) (PαMSAN) [6]].

Compared with selective localization within one phase, localization of GNPs at the interface can further reduce the percolation threshold and enhance the electrical conductivity of the polymer composite. By either modifying the filler surface energy [7] or designing compounding sequences [8,9], individual graphene or graphene oxide sheets can effectively tile at immiscible fluid interfaces and form particle network assemblies, thereby achieving global percolation at lower particle concentration. Nevertheless, chemical functionalization of GNPs is usually difficult to control, more labor intensive, and creates defects on the delocalized π-electron system that lower the filler electrical conductivity. Therefore, it is preferable to use unmodified GNPs. We have shown that it is possible to achieve interfacial filler localization through a controlled two-step compounding sequence [9,10].

The general strategy is as follows: the fillers are initially compounded with the thermodynamically unfavorable

[a]Authors to whom correspondence should be addressed; electronic mail: xcheng@umn.edu and macosko@umn.edu

polymer component into a masterbatch. Then, the masterbatch is melt compounded with the favorable component. Interfacial filler localization is achieved during the second compounding step by either thermodynamic or kinetic trapping. In thermodynamic trapping, surface wetting conditions determine the interfacial localization of the fillers through the minimization of global free energy. Therefore, during the second compounding step, the fillers previously located in the unfavorable polymer phase will transfer to the interface due to neutral wetting conditions with the wetting coefficient ω between −1 and 1 as discussed below [8,11]. In kinetic trapping, even though the global free-energy minimum is reached when the filler particles localize in the preferred polymer phase, the interface can create a local energy well deeper than the thermal energy of fillers and kinetic energy of convective mixing. Therefore, interfacial filler localization can be achieved by controlling kinetic parameters such as the melt compounding time [9].

In Table I, we review the literature that has achieved interfacially localized graphene sheets in cocontinuous polymer blends using the two-step compounding sequence. The two-step compounding sequence has been applied to carbon-based fillers of different geometries, i.e., CB (spheres, 3D) [12–16], graphene (platelets, 2D), and carbon nanotube (CNT, rods, 1D) [17–22], to create conductive blends with interfacially localized fillers. GNPs when localized at the interface of polymer blends are preferred to CBs or CNTs. CBs have much smaller lateral dimensions (tens of nm) as compared to the lateral dimensions of GNPs or lengths of CNTs (hundreds of nm). Thus, CBs require much higher percolation thresholds as compared to CNTs or GNPs in polymer blends: typical percolation thresholds of CBs when selectively localized at the cocontinuous interface are ∼5–10 wt. % [16]. However, careful optimization of the particle dispersion, blend compounding, and post-processing conditions such as annealing time and temperature can further reduce the percolation threshold to ∼0.4 wt. % in a polyethylene (PE)/PS system, achieving an electrical conductivity of $\sim 10^{-3}$ S/cm at 1 wt. % CB concentration [13]. On the other hand, CNTs exhibit faster interfacial transfer characteristics and lower interfacial stability as compared to CBs or GNPs, according to the slim-fast mechanism proposed by Göldel *et al.* [23]. In addition, CNTs are 1D rods and do not tile interfaces as efficiently as 2D platelets. As such, typical percolation threshold of interfacially localized CNTs is ∼0.7 wt. % [22]. A different approach by Chen *et al.* [19] created interfacially localized CNTs in PC/acrylonitrile-butadiene-styrene (ABS) immiscible blends by adding 5 wt. % of a third polymer, maleic anhydride-grafted ABS (ABS-*g*-MA), as compatibilizer. In their approach, CNTs were predispersed with ABS-*g*-MA into a masterbatch, then melt compounded with PC and ABS to obtain a quaternary composite. They achieved an ultralow, ∼0.05 wt. % percolation threshold, with an electrical conductivity of $\sim 10^{-7}$ S/cm at 1 wt. % CNT concentration.

Interfacially localized particles might be expected to be unstable under flow, particularly when they are in nonequilibrium systems such as immiscible polymer blends. Nevertheless, there has been no previous report that characterizes the processing stability of the percolated conductive particle network localized at the interface of cocontinuous polymer blends. In melt processes such as extrusion, calendaring, and injection molding, conductive polymer composites are subject to nonlinear shear and extensional deformations. Therefore, understanding whether interfacial GNP networks in cocontinuous polymer blends are robust to withstand processing flows and maintain their interfacial localization and electrical conductivity is important for future applications of this class of polymer/GNP composites.

In this work, we successfully achieve interfacial localization of GNPs in an immiscible blend of commercial PLA and poly(ethylene-*co*-vinyl acetate) (EVA). Our system exhibits good melt processability and favorable mechanical properties for practical applications; ductility of EVA compensates for

TABLE I. Blends with interfacial GNP or r-GO (reduced graphene oxide).

Material system and compounding sequence	Year	Estimated percolation threshold (wt. %)	Electrical conductivity (S/cm) at 0.5 wt. % filler concentration[d]	Reference
(SAN/GNP)/PC	2013	n/a	n/a	Liebscher *et al.* [4]
(PLA/GNP)/PCL	2016	0.23[c]	n/a	Huang *et al.* [24]
(PLA/r-GO)/EVA[a]	2017	0.18	$\sim 10^{-9}$ (25 °C)	Shen *et al.* [25]
(PP/r-GO)/PE[b]	2017	1.81[c]	n/a	Tu *et al.* [26]
(PLA/r-GO)/PS[b]	2017	0.062[c]	$\sim 10^{-6}$ (180 °C)	Bai *et al.* [8]
(PLA/GNP)/PS	2018	<0.5	$\sim 10^{-4}$ (180 °C); $\sim 10^{-6}$ (25 °C)	Bai *et al.* [9]
(PLA/GNP)/HDPE	2019	0.11–0.22[c]	$\sim 10^{-8}$–10^{-7} (25 °C)	Mun *et al.* [10]
(LLDPE/GNP)/EVA	2019	0.77[c]	n/a	Helal *et al.* [27]
(POE/GNP)/PA6	2020	0.66	n/a	Hadaeghnia *et al.* [28]
(PLA/GNP)/EVA	2021	0.048	$\sim 10^{-5}$ (170 °C)	this work

[a]Chemically reduced graphene oxide.
[b]Thermally reduced graphene oxide.
[c]Weight fraction (W_f) values are converted from volume fraction (V_f) in the original references, using $W_f = \rho_f V_f/(\rho_f V_f + \rho_m(1 - V_f))$. The density of the graphene filler and polymer matrix are assumed to be $\rho_f = 2.2\,\mathrm{g/cm^3}$ and $\rho_m = 1.0\,\mathrm{g/cm^3}$, respectively, which may be a potential source of error due to the density difference between different polymer species and between GNPs and r-GO.
[d]Measurement temperature noted in parentheses.

the intrinsic brittleness of PLA. Wetting property analysis indicates that the interfacial localization of GNPs results from kinetic trapping in our system. Using the prescribed two-step melt compounding sequence, we achieve an ultra-low GNP percolation threshold of ~0.048 wt. %. Interfacial GNP localization is confirmed by transmission electron microscopic (TEM) imaging and rheology. The electrical conductivity of our system at 0.10 wt. % GNP concentration reaches $\sim 10^{-7}$ S/cm when measured at 170 °C. The electrical conductivity demonstrated by the current system is one of the highest compared to other published works at comparable filler concentrations (Table I) and falls in the range of electrostatic discharge protection materials (10^{-4}–10^{-11} S/cm) [29].

We also characterize the strength of the interfacial GNP network in response to different processing flow conditions using rheology in both linear and nonlinear regimes. The rheological study is supported by TEM imaging that compares system morphology before and after nonlinear flows. Our results suggest that the interfacial GNP network produced by kinetic trapping via controlled compounding is robust against moderate shear and extensional flow conditions typically encountered in conventional material processing. Moreover, high conductivity is maintained during 2–10 min melt compounding. Taken together, our study demonstrates the feasibility to kinetically trap graphene at the interface of cocontinuous PLA/EVA blends, yielding electrically conductive composites whose conductive particle network is robust during melt processes. Such a method may potentially be adapted to manufacture cocontinuous conductive polymer composites of many other immiscible polymer blend systems.

II. EXPERIMENTS

A. Two-step compounding of the polymer composites

1. Material

PLA (Ingeo 4032D, $M_w = 117\,500$ g/mol, $Đ = 1.86$) and EVA (Elvax 40 W, 40 wt. % vinyl acetate, $M_w = 17\,400$ kg/mol, $Đ = 3.06$) pellets were obtained from NatureWorks and DuPont, respectively. Both polymers were dried *in vacuo* at 40 °C at least overnight before compounding to remove residual moisture. Molecular weight characterizations were performed via size-exclusion chromatography (Fig. S1 and Table S1 in the supplementary material [60]). GNPs (N002-PDR, $\rho = 2.2$ g/cm^3) were obtained from Angstron Materials and used as received. According to previous reports and our TEM observations, the average lateral dimension of GNPs was ~1.5 μm and the average thickness was ~1.0–1.2 nm, corresponding to an approximately three-layer stack of graphene sheets [5,9,10,30].

2. Masterbatch preparation

The PLA/EVA/GNP ternary composites were prepared using a two-step compounding sequence, for which a homopolymer/GNP masterbatch is prepared by solution blending and probe sonication. GNPs were dispersed into tetrahydrofuran (THF, reagent grade, Sigma-Aldrich) at a concentration of <2 mg/ml. The suspension was probe sonicated (Branson Digital Sonifier SFX 250, 1/4 in. diameter probe) continuously for 1 h at 75 W in an ice-water bath to break up large aggregates of GNPs. In a separate beaker, the homopolymer was dissolved in THF at a concentration of 1 g/10 ml. The polymer/THF solution was combined with the GNP/THF suspension at the desired polymer/graphene concentration and stirred for ~5 min before co-precipitated into ~500 ml of methanol. The precipitate appeared homogeneous and gray in color, and the supernatant solution was clear, suggesting all GNPs transferred from the solvent into the polymer phase. The product was collected and dried *in vacuo* at 60 °C overnight and melt compressed for 5 min at 170 °C to form ~3 mm thick sheets for subsequent compounding. The current approach of masterbatch preparation is limited by the batch size since it requires using large amounts of volatile solvents (THF and methanol) to dissolve and precipitate polymers. In addition, probe sonication in GNP/THF suspension was necessary to ensure good GNP dispersion in the polymer matrix for high electrical conductivity. As a result, the method may not be immediately viable for scaled-up production.

3. Melt compounding

The ternary composites were prepared by melt compounding using a 5 ml benchtop conical twin-screw microcompounder (DSM Xplore MC5). Nitrogen purge gas was used during melt compounding to mitigate the effect of oxidative degradation. During melt compounding, a total of ~5 ml of polymer/GNP masterbatch and the other homopolymer were loaded into the microcompounder at 180 °C operating at 100 rpm. The processing temperature of 180 °C is chosen to ensure PLA is fully amorphous and not undergo thermal degradation or molecular weight reduction during melt compounding. The specific mechanical energy of the melt compounding process is estimated to be at least ~108 kJ/kg min (Fig. S2 in the supplementary material [60]) based on prior literature [31]. Typical loading times were ~5 min, and the mixing time was varied between 1 and 20 min. Apart from the mixing time studies (see below), compounding time was fixed at 2 min as it was sufficient to produce blends with the highest electrical conductivity. The ternary composite was then extruded from the compounder in ~3 min, and the morphology was frozen by rapidly quenching in air.

B. Blends characterization

1. Transmission electron microscopy

Polymer composite samples for TEM were prepared by ultramicrotomy (Leica EM UC6) at −140 °C with a diamond knife. Ultrathin sections with nominal thicknesses of 65–85 nm were loaded onto copper grids carefully using an eyelash. Bright-field TEM imaging was performed on a FEI Tecnai G2 Spirit BioTWIN microscope equipped with a LaB_6 emission source and operating at an accelerating voltage of 120 kV. Images were captured with an Eagle 4 megapixel CCD camera.

2. Scanning electron microscopy

Scanning electron microscopy (SEM) was used to verify the cocontinuity of the polymer phases after melt compounding. The EVA phase was chemically etched out using cyclohexane (reagent grade, Sigma Aldrich) at 50 °C for 24 h. Then, the remaining sample was carefully removed from the solvent, allowed to air dry for 1 h, and sputter coated with 5 nm of Pt (Leica EM ACE600). The microstructure of the remaining composite scaffold was characterized using a Hitachi SU8230 SEM. Images were obtained at an accelerating voltage of 3.5–5.0 kV.

3. Rheology and electrical conductivity

Prior to the testing, the polymer composites were compression molded into 0.75 mm thick sheets using a hot press (Wabash Carver Press) at 180 °C and ~9 MPa pressure. To prevent excessive domain coarsening prior to rheological characterization, the compression molding time was controlled to be no more than 2 min. Then, the samples were rapidly quenched in a separate hydraulic press with cooling water to freeze the morphology. Finally, samples were cut using either a circular die or a razor blade into desired shapes according to the type of rheological characterization of interest. Shear rheology was measured with an ARES 2 rheometer equipped with a dielectric thermal analysis accessory (TA Instruments) and 25 mm-diameter dielectric parallel plates. Dielectric shear rheology allowed the simultaneous measurement of rheology and electrical conductivity during shear deformation, as shown in our previous work [5,8,10]. Unless specified, all electrical conductivities were measured at the AC frequency $\omega_{AC} = 20$ Hz, which approximates the DC conductivity (further discussion of AC frequency-dependent conductivity data is provided in Fig. S3 in the supplementary material [60]). Extensional rheology was measured with an ARES-G2 rheometer (TA Instruments) with the extensional viscosity fixture (EVF). Samples were cut into ~120×10 mm^2 rectangular pieces, then loaded onto the test geometry whose temperature was equilibrated at 170 °C in the convection oven. After ~30 s of temperature re-equilibration, samples were subject to a constant extension rate until sample failure. Using the liquid nitrogen-based cooling system in the convection oven, samples were rapidly quenched immediately after either startup of shear or extension. Sample regions with the highest strain (i.e., around the edge of the circular disc in shear flow or around the breaking point in extensional flow) were embedded in an epoxy resin to allow TEM sample preparation.

III. RESULTS AND DISCUSSION

A. Controlled two-step compounding sequence produces interfacial graphene

1. Wetting coefficient analysis

Localization of fillers in a polymer blend is determined by the pairwise interfacial energies of the system, using Young's equation [5,8,9],

$$\omega = \cos\theta = \frac{\gamma_{PLA/GNP} - \gamma_{EVA/GNP}}{\gamma_{PLA/EVA}}. \quad (1)$$

For the present system, thermodynamically GNP prefers localization in the EVA phase if $\omega > 1$, the PLA phase if $\omega < -1$, and at the PLA/EVA interface if $-1 < \omega < 1$. The pairwise interfacial energies in this study are calculated using the Owens–Wendt equation with the dispersive and polar components of the surface energy of pure components,

$$\gamma_{A/B} = \gamma_A + \gamma_B - 2\sqrt{\gamma_A^d \gamma_B^d} - 2\sqrt{\gamma_A^p \gamma_B^p}. \quad (2)$$

The surface energies of EVA and PLA polymers are obtained from the literature, based on sessile drop contact angle measurements [32]. The values are further corrected to the processing temperature at 180 °C. From experimentally obtained surface energies of pure GO [33] and chemically reduced GO [34], we extrapolate the surface energy of GNPs under the assumption that γ^d is not significantly affected by the C/O ratio while γ^d/γ^p is proportional to the C/O ratio. Based on the manufacturer's datasheet and consistent with previous studies [5], the GNPs used in this study have a C/O ratio of 50.7. We provide surface energies of the pure components in Table S2 in the supplementary material [60]. Using Eq. (2), we calculate γ, γ^d, and γ^p of GNP at 180 °C to be 29.4, 29.0, and 0.4 mN/m, respectively. Therefore, the calculated $\gamma_{PLA/EVA}$, $\gamma_{PLA/GNP}$, and $\gamma_{EVA/GNP}$ at 180 °C are 4.1, 8.7, and 1.4 mN/m, respectively. Based on Young's equation, the wetting coefficient $\omega = 1.8$. We repeated our calculation using two additional references for the surface energy of PLA (see Table S2 in the supplementary material [60]). The calculated ω is found to range between 1.8 and 3.1. Since the analysis based on each set of surface energy values yields $\omega > 1$, GNPs should thermodynamically localize in the EVA phase. Informed by the analysis, the two-step melt compounding sequence is designed such that we initially prepare a PLA/GNP masterbatch, followed by melt compounding it with the EVA homopolymer. During the second compounding step, GNPs that transfer from the thermodynamically less favorable PLA phase to the more favorable EVA phase become kinetically trapped at the PLA/EVA interface.

2. Blend morphology obtained by kinetic trapping

GNP localization is demonstrated via TEM (Fig. 1). In TEM images, GNPs are shown as thin, dark lines which reflect their high geometric aspect ratio and high electron density. The light gray and dark gray phases are attributed to PLA and EVA domains, respectively, from mass-thickness contrast. Previous reports show that PLA undergoes degradation under electron beam irradiation [35], whereas EVA is known to be resistant to electron beam damage [36]. For all three images, GNP concentration is fixed at 0.5 wt. %. Figures 1(a) and 1(b) show the morphology of the (PLA/GNP)/EVA blend created using the two-step compounding sequence that enables kinetic trapping of GNP at the PLA/EVA interface. Based on low magnification images [Fig. 1(b) and Figs. S4(a) and S4(b) in the supplementary material [60]], the overall blend morphology is cocontinuous. A large number of GNPs localize at and align with the PLA/EVA interface, forming an interconnected particle network.

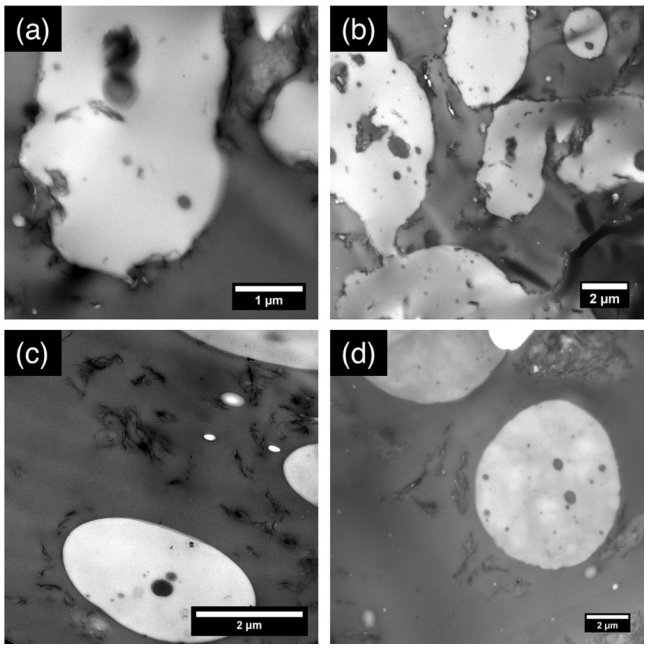

FIG. 1. TEM images of ternary composite samples obtained from different processing sequences, showing direct contrast among the components: PLA (light gray domains), EVA (dark gray domains), and GNP (thin, black lines). Two-step melt compounding: (a) and (b) (PLA/GNP)/EVA; (c) PLA/(EVA/GNP). Single-step melt compounding: (d) PLA/EVA/GNP. Interfacial GNP localization is achieved only in the (PLA/GNP)/EVA system. For all blends, the PLA/EVA compositions are 50/50 wt. % and GNP concentrations are 0.5 wt. %.

Some GNPs have fully migrated into the EVA phase, whereas very few GNPs remain in the PLA phase. In these images, GNPs appear randomly dispersed and the PLA/EVA interfaces do not show anisotropy.

In contrast, blends created from either the reversed two-step compounding sequence [i.e., PLA/(EVA/GNP), Fig. 1(c)] or one-step compounding sequence [i.e., PLA/EVA/GNP, Fig. 1(d)] show droplet-matrix morphologies where GNPs localize exclusively in the EVA phase. No GNP is observed in either the PLA phase or at the interface. These results agree with the wetting coefficient calculations with $\omega > 1$. Furthermore, in (PLA/GNP)/EVA systems, GNPs localized at the PLA/EVA interface result in irregular domains and nonuniform interfacial curvatures. This is in contrast with the PLA/(EVA/GNP) or PLA/EVA/GNP systems, where the PLA droplets have regular spheroidal shapes and uniform interfacial curvatures.

The bulk cocontinuity of the composite is further demonstrated by SEM imaging, complementing the 2D TEM images. The EVA phase is selectively extracted using cyclohexane at 50 °C for 24 h. Figure 2 shows the 3D morphology of the remaining 50/50 (PLA/GNP)/EVA blends with 0.5 wt. % GNPs and 2 min melt compounding time. After solvent extraction, the structure of the remaining blend remained intact. Low magnification images show the remaining PLA phase is continuous throughout the field of view [Figs. 2(a) and 2(b)], supporting our conclusion based on the TEM images. After solvent extraction, some GNPs were found in the cyclohexane phase as they were previously localized EVA phase. Nonetheless, high magnification SEM image shows the presence of interfacially localized GNPs at the surface of PLA domains [Fig. 2(c)], which act to stabilize the cocontinuous blend morphology.

3. The effect of compounding time on the blend morphology

Controlling the time of the second melt compounding step is essential for kinetically trapping GNPs at the PLA/EVA interface during melt processing. Thermal energy alone is insufficient to induce GNP migration over significant distances. Following prior work [5], we assume the hydrodynamic radius (R_h) of GNPs in this study to be ~450 nm. Thus, the typical diffusion length (d) of individual GNP sheet over 10 min of compounding time (t) can be estimated using Einstein's equation,

$$d = \left(\frac{tkT}{\pi\eta R_h}\right)^{\frac{1}{2}}, \tag{3}$$

where k is the Boltzmann constant, $T = 180\,^{\circ}C$ is the processing temperature, and η is the melt viscosity of the polymer ($\eta_{PLA} = 6500$ Pa s and $\eta_{EVA} = 300$ Pa s at 180 °C). According to our estimation, $d_{PLA} = 20$ nm and $d_{EVA} = 95$ nm, both of which are well below the average domain size of either the PLA or EVA phase. Instead, GNPs are driven to interfaces by the high shear and extension rates encountered during twin screw microcompounding [37].

However, longer compounding flow times can further drive kinetically trapped GNP sheets at the interface into the thermodynamically preferred phase. The PLA/EVA interface is constantly pinched off and folded over itself due to compounding flow. Thus, interfacial GNP sheets can be fully encapsulated in the EVA phase due to the constant stretching and folding of the interface during longer compounding times [9]. Therefore, determining the appropriate time window for the second melt compounding step is necessary to achieve the optimal interfacial localization. We measure the electrical conductivity of the 50/50 (PLA/GNP)/EVA_0.5 wt. % system after different melt compounding times ($t_{cmpd.}$) (Fig. 3). Our data show that when $t_{cmpd.} \leq 1$ min, the electrical conductivity is low, suggesting that the melt compounding time is not sufficient to drive most of the GNPs to the PLA/EVA interface. This is confirmed by both selective solvent extraction experiments and TEM imaging. After performing solvent extraction of the EVA phase on a sample with identical blend composition and GNP concentration but prepared with $t_{cmpd.} = 1$ min, the blend disintegrated completely. TEM imaging shows that the overall blend morphology was droplet-matrix with EVA being the matrix phase (Fig. S5 in the supplementary material [60]). Even though a small fraction of GNPs has migrated to the interface, a large fraction of GNPs remained in the PLA phase. These results suggest that $t_{cmpd.} \leq 1$ min is insufficient to create cocontinuous morphology where a large fraction of GNPs transfer to the interface. When 2 min $\leq t_{cmpd.} \leq 10$ min, the electrical conductivity is high, suggesting that most of the GNPs have already been kinetically trapped at the interface forming a percolated conducting network. This is consistent with TEM observations [Fig. 1(a)], as GNPs are largely absent

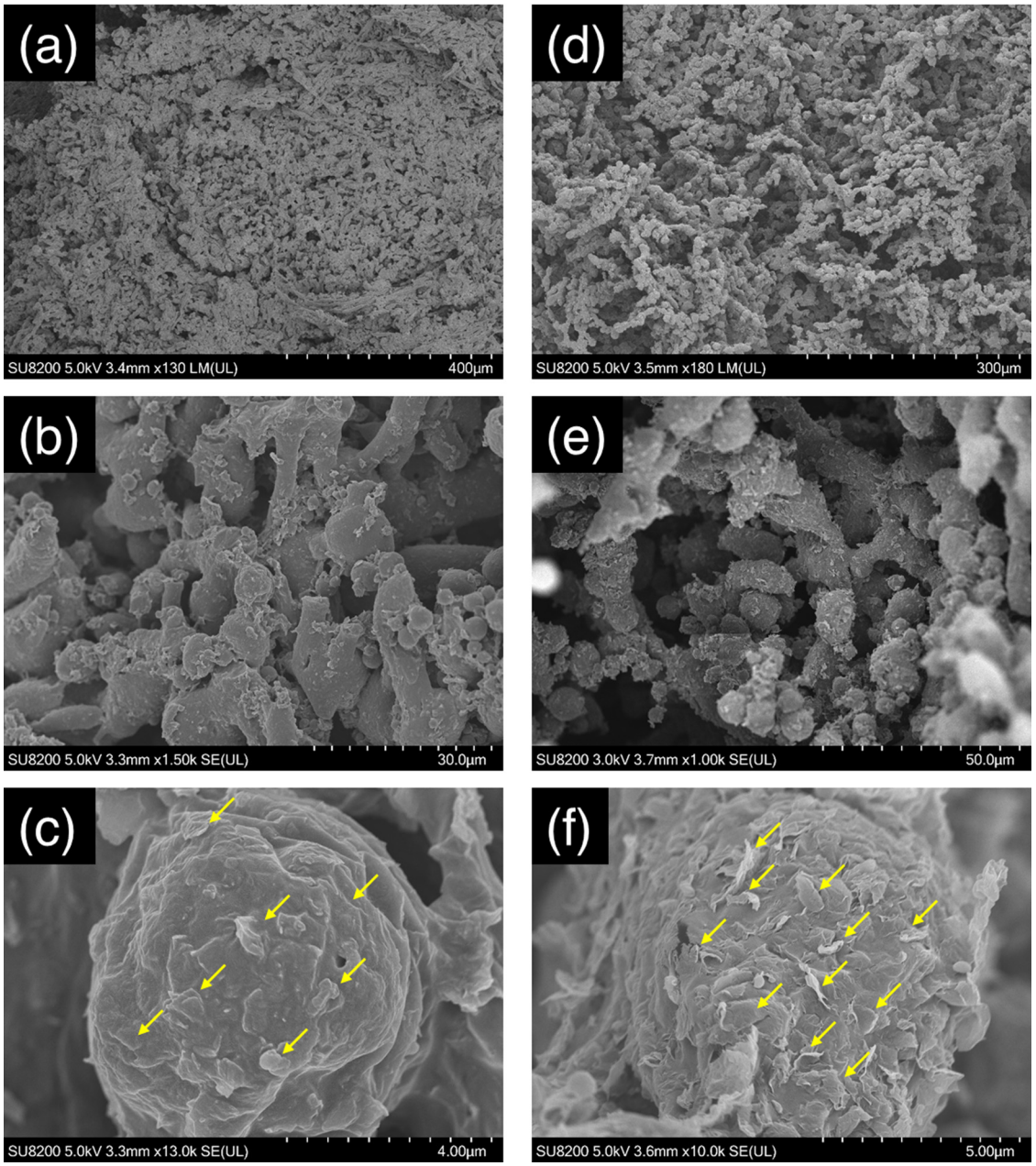

FIG. 2. SEM image of 50/50 (PLA/GNP)/EVA_0.5 wt. % with 2 min [(a)–(c)] and 5 min [(d)–(f)] melt compounding time. The EVA phase was selectively extracted by cyclohexane. The remaining PLA phase was continuous. GNPs were found at the surface of the remaining PLA domains, suggesting the kinetic trapping of GNP at the PLA/EVA interface. GNPs on the surface of PLA domains are marked by yellow arrows in (c) and (f).

in the PLA phase when $t_{cmpd.} = 2$ min. SEM imaging of a sample with $t_{cmpd.} = 5$ min after selective EVA phase removal further demonstrates the bulk morphology of the polymer blend is cocontinuous [Figs. 2(d) and 2(e)] and GNPs achieve good interfacial coverage [Fig. 2(f)]. Finally, when $t_{cmpd.} = 5$ min, the electrical conductivity decreased, suggesting that a significant number of GNPs have migrated into the EVA phase. This is confirmed in Fig. S6 in the supplementary material [60]: after applying shear for 120 s at 1 s^{-1} shear rate, some GNPs previously localized at the interface have transferred to the EVA phase. The blend morphology after shear is less cocontinuous since the polymer domains are broken into droplets by applied shear. For the above reasons, we select $t_{cmpd.} = 2$ min as the optimal compounding time, which is already sufficient for most GNPs to be kinetically trapped at the interface. Furthermore, the electrical conductivity shows only a slight increase over 1 h of isothermal annealing for all samples (Fig. S7 in the supplementary material [60]). Since an increase in electrical conductivity is usually attributed to microscopic structural recovery of the elastic GNP network [38], our results further suggest that thermal energy alone does not significantly affect the GNP localization after kinetic trapping has occurred.

Even though the blends are subject to high rates of deformation during melt compounding, GNPs remain trapped at the interface as confirmed by nonlinear rheology and TEM imaging (see below). As shown in Fig. 3, electrical conductivities remain high for a range of compounding

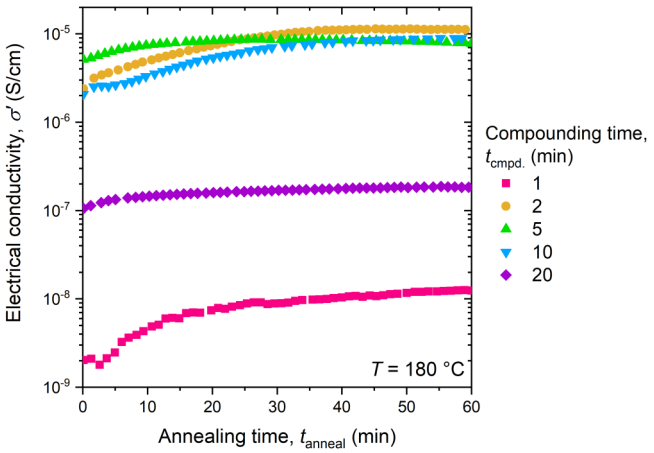

FIG. 3. The effect of different melt compounding times on the electrical conductivity of 50/50 (PLA/GNP)/EVA_0.50 wt. % blends. The electrical conductivities are measured continuously with the dielectric rheology accessory during isothermal annealing at 180 °C. The electrical conductivities of blends with 2–10 min of compounding time are substantially higher than those with either smaller or longer compound times, suggesting GNPs formed well-connected interfacial networks within the 2–10 min compound time window. One hour annealing slightly improves the electrical conductivities of blends.

times of 2–10 min. The PLA/EVA system shows higher stability of interfacial GNPs compared with our previous studies of kinetic trapping using other polymer blends: the optimal compounding time was only 30 s for PLA/PS blends [9] and 5 min for HDPE/PLA blends [10]. Kinetic factors provide energy barriers that prevent the full GNP migration from the PLA/EVA interface to the EVA phase. These factors could include the rate of adsorption-desorption of polymer chains on the GNP surface [24,39], the resistance of adjacent graphene sheets from the particle network [8], and the low rate of migration of GNPs oriented parallel to the interface [9]. Since these kinetic factors depend on specific polymer systems, this could explain why the optimal compounding time for the PLA/EVA system is different from our previously studied systems.

The morphology created by kinetic trapping of GNPs at the interface is stable. Fillers suitable for kinetic trapping need to exhibit a local energy barrier, which prevents individual graphene sheets from leaving the interface [9,10]. Figure 4 is a schematic that illustrates the four key stages of filler migration from one phase to another phase: (1) bulk migration far from the interface, (2) film drainage of the departing phase at the interface, (3) the displacement of the three-phase contact line at the filler surface, and (4) eventual particle migration across the interface and fully into the thermodynamically preferred phase [40]. The first two stages are not rate-limiting steps of kinetic trapping. For (1), convective flow by melt compounding is sufficient to transfer GNPs from the PLA phase toward the interface. For (2), since TEM images [Figs. 1(a) and 1(b)] already indicate the presence of interfacial GNPs after 2 min of melt compounding, the film drainage time on the filler surface is much shorter than their contact time at the interface. The rate of filler migration across the interface, which is determined by (3), is the rate-limiting step that determines the effectiveness of kinetic trapping. When the filler contacts with the interface and forms the three-phase contact line, the rate of particle migration across the interface is equal to the displacement velocity (V) of the three-phase contact line,

$$V = \frac{F}{\xi L}. \tag{4}$$

Here, F is the thermodynamic driving force to minimize the overall interfacial energy, ξ is the friction coefficient which scales with the viscosities of the two polymer phases [41,42], and L is the length of the three-phase contact line. Equation (4) shows that the rate of GNPs migration near the interface is orientation dependent. While both F and ξ are the same for GNPs regardless of orientation, $L \sim 1$ μm for GNPs oriented parallel with the interface while $L \sim 1$ nm for GNPs oriented perpendicular to the interface. Therefore, the migration rate of GNPs oriented parallel with the interface is $\sim 10^3$ slower than the rate of those oriented perpendicular to the interface. Consequentially, the migration of interfacial GNPs oriented parallel with the interface will be arrested upon cessation of processing flow. We believe kinetic trapping is most effective for nanoparticles with platelet-type geometries such as GNPs to create blends with stable interfacial particles: GNPs' high aspect ratio allows them to tile interfaces efficiently and achieve a lower percolation threshold than low aspect ratio fillers such as CB. Compared to 1D nanorods such as CNTs, the 2D platelet geometry of GNPs implies a slower rate of filler migration and higher interfacial stability according to the slim-fast mechanism [23].

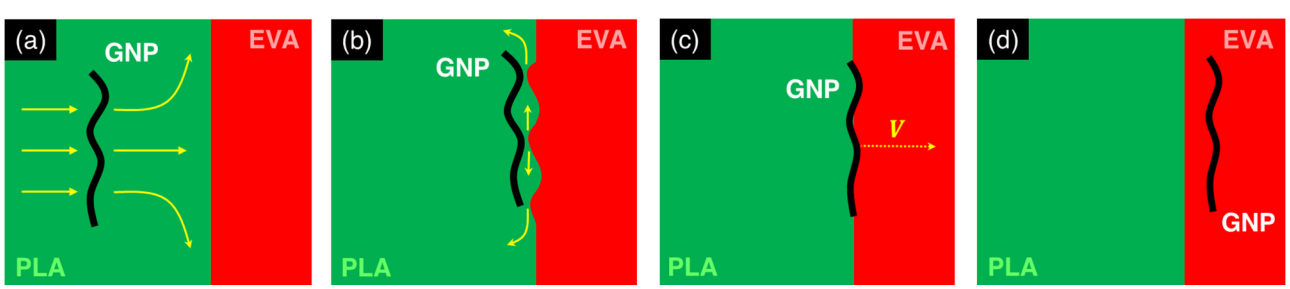

FIG. 4. Schematic showing the four stages of GNP migration from the PLA phase to the EVA phase: (a) bulk migration far from the interface, due to convection by the compounding flow with the background PLA matrix, (b) film drainage of the departing phase at the interface, induced by the attractive interactions between GNP and EVA, (c) the displacement of the three-phase contact line at the filler surface, and (d) eventual particle migration across the interface into the preferred EVA phase.

B. Interfacial graphene affects rheology and conductivity

As shown from TEM, the interfacial GNP networks formed by the two-step compounding sequence cover the cocontinuous PLA/EVA interface. Rheological and conductivity measurements of the ternary composite confirm these observations. Specifically, we study the effects of the interfacial GNP network on the composite's elastic modulus (G') and real part of the complex electrical conductivity (σ') when either linear or nonlinear deformation is applied.

1. Linear viscoelasticity

Measuring G' using small amplitude oscillatory shear in the linear viscoelastic region provides insights into the state of nanoparticle dispersion and localization within polymer blends. For a ternary polymer/graphene composite, there are three components that contribute to the overall G',

$$G' = G'_{\text{mat}} + G'_{\text{int}} + G'_{\text{GNP}}, \tag{5}$$

where G'_{mat}, G'_{int}, and G'_{GNP} represent the contribution from the polymer matrix, interface, and GNPs respectively. As shown in Fig. 5(a), G'_{mat} of either PLA or EVA homopolymers at 170 °C shows classic terminal behavior, $G' \sim \omega^2$, where ω is the oscillation frequency. In the case of the PLA/EVA homopolymer blend, the interface contributes to additional elasticity of G'_{int}, which results in an apparent flattening of the G' vs ω profile in the terminal region. Finally, when GNPs are added to the polymer blend system, the filler particles contribute further to the overall elasticity in the terminal flow region.

We compare G' of two ternary composite samples with the same polymer composition (50/50 wt. %) and GNP concentration (0.5 wt. %) but with the reverse compounding sequence. Results show that the (PLA/GNP)/EVA sample exhibits ~4 times higher G' as compared to the PLA/(EVA/GNP) sample, suggesting that the bulk connectivity of GNPs is better in the (PLA/GNP)/EVA sample as compared to the PLA/(EVA/GNP) sample. Specifically, the (PLA/GNP)/EVA sample displays a clear plateau (i.e., $G' \sim \omega^0$) in the terminal flow region, suggesting the formation of a solid-like, interconnected GNP network that percolates throughout the entire composite. Rheological percolation is also detected by replotting the dynamic frequency sweep data as Cole-Cole plots (i.e., imaginary part vs real part of complex viscosity, η'' vs η'). In Fig. 5(b), Cole-Cole plots of the homopolymers show a single relaxation spectrum in the shape of a circular arc. The PLA/EVA neat blend shows a slight uptick, representing the additional relaxation of dispersed PLA droplet phase. For the blends containing GNPs, the Cole-Cole plots reflect the rheological percolation of the GNP network, which is formed either at the PLA/EVA interface for the (PLA/GNP)/EVA system or in the continuous EVA phase for the PLA/(EVA/GNP) system. The effect of particle percolation is much stronger than either the relaxation of polymer chains or the dispersed droplets [43]. Finally, the small amplitude oscillatory shear results are consistent with TEM observations [Figs. 1(a) and 1(b)], in which a large fraction of GNPs localize at the PLA/EVA interface forming a percolating particle network.

The dielectric accessory enables measurements of the composites' electrical conductivity, which further elucidate the characteristics of the GNP network formed as a result of different compounding sequences. In Fig. 6, the real part of the complex conductivity is plotted as a function of GNP concentration for both homopolymer/GNP blends and the two ternary composites. Two key observations are drawn from these results. First, below 1 wt. % GNP concentration the conductivity of the ternary composites is higher than the homopolymer/GNP composites. The selective localization of GNP in the EVA phase or at the interface of the cocontinuous blend reduces the percolation volume of the fillers [5,6]. Second, the (PLA/GNP)/EVA composites with interfacial GNPs have the highest electrical conductivity. Since the GNPs have a two-dimensional planar geometry, interfacially localized GNPs cover the cocontinuous polymer interface and result in a much lower percolation threshold as compared to

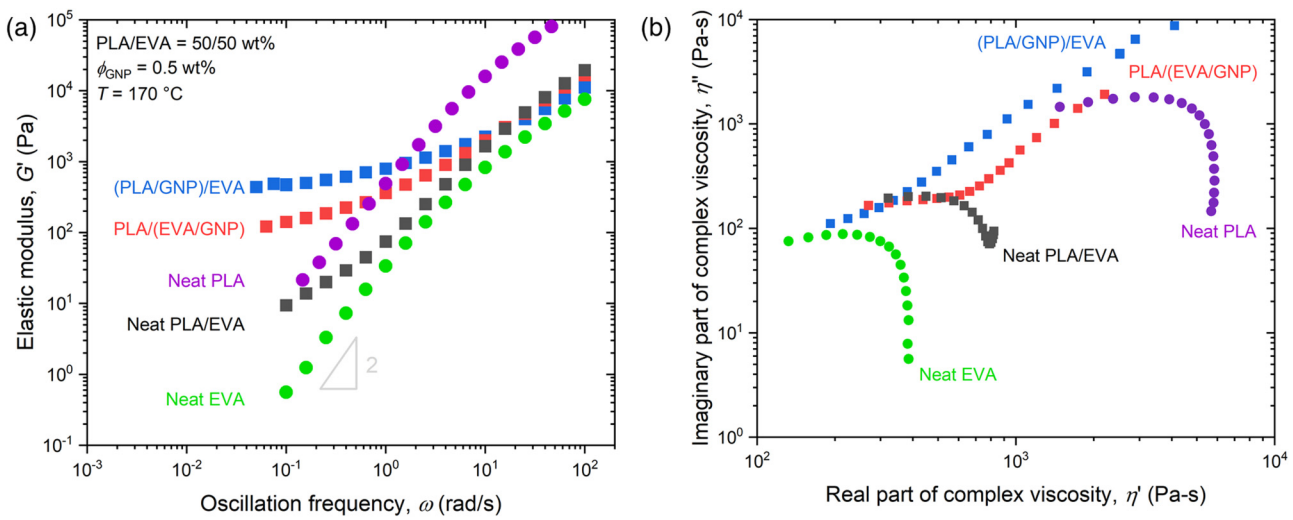

FIG. 5. Dynamic frequency sweep results shown as (a) elastic moduli vs oscillation frequency and (b) Cole-Cole plots for homopolymers, 50/50 wt. % PLA/EVA neat blends, and 50/50 PLA/EVA/GNP blends produced with different compounding sequences.

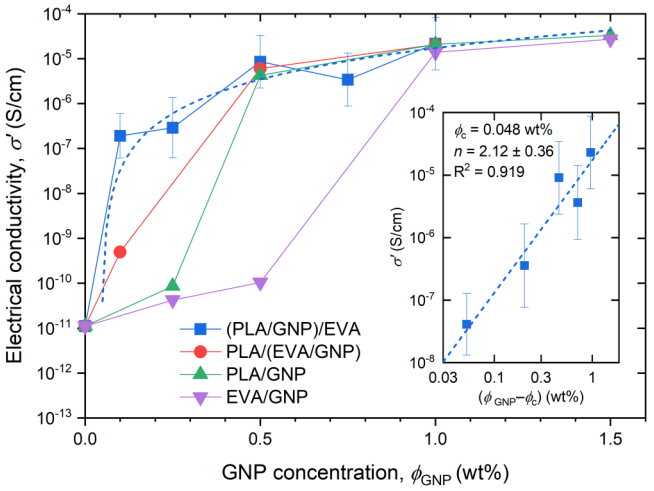

FIG. 6. Electrical conductivity as a function of GNP concentration for various polymer composite systems measured at 170 °C. The inset shows a sample power law fitting of the percolation threshold of the (PLA/GNP)/EVA blend.

GNPs localizing in a three-dimensional polymer matrix phase. We conduct measurements at 170 °C immediately after the conclusion of the dynamic frequency sweep experiments (~20 min) so that the annealing times across samples are consistent and any residual stress from prior processing is fully relaxed.

The percolation threshold refers to the minimum concentration of GNPs in the system to form a fully connected particle network spanning throughout the composite. Above the threshold, a sharp insulator-to-conductor transition is expected. The transition can be estimated from the classical percolation theory model given by

$$\sigma = A\,(\phi_{\mathrm{GNP}} - \phi_c)^n, \tag{6}$$

where σ is the electrical conductivity of the composite, ϕ is the GNP concentration, ϕ_c is the percolation threshold of GNP, n is the critical exponent that relates to the aspect ratio and spatial distribution of the fillers [44], and A is the exponential prefactor. The percolation thresholds of each set of polymer/GNP composites are calculated by fitting the results to Eq. (6). The power law fitting curve for the (PLA/GNP)/EVA blend is shown in the inset of Fig. 6; similar plots for the control samples are provided in Fig. S8 in the supplementary material [60]. The results are summarized in Table II. The percolation threshold of PLA/(EVA/GNP) where GNPs localized in only the EVA phase sees a roughly twofold decrease from either homopolymer/GNP composite, which agrees with our hypothesis that the GNP percolation volume is approximately halved. More notably, in the (PLA/GNP)/EVA samples where a majority of GNPs localize at the PLA/EVA interface, an ultralow percolation threshold of 0.048 wt. % (~0.022 vol. %) GNPs is attained, representing a ninefold reduction from the systems consisting of homopolymer/GNP composites.

TABLE II. Percolation thresholds of polymer/GNP composites of different polymer composition and compounding sequences.

Sample	ϕ_c (wt. %)	n
50/50 (PLA/GNP)/EVA	0.048	2.12
50/50 PLA/(EVA/GNP)	0.229	1.18
PLA/GNP	0.436	0.73
EVA/GNP	0.601	0.82

2. *Transient shear rheometry*

While the linear viscoelastic behavior of the composites demonstrates that a connected interfacially localized GNP particle network can be formed by the two-step compounding sequence, these measurements do not offer insights into the robustness of the GNP network when subject to stronger flows. Conductive polymer composites are usually melt processed by extrusion, calendaring, or injection molding, all of which produce much higher strains and strain rates in both shear and extension. Therefore, we studied whether the GNP network at the cocontinuous PLA/EVA interface maintains good particle interconnectivity and preserves the bulk electrical conductivity when the composite is subject to large deformations. To address this question, we utilized a series of nonlinear shear and extensional rheology coupled with either dielectric measurements or TEM imaging to understand how the interfacial GNP network responds to nonlinear deformation.

For nonlinear shear deformations, we perform a series of startup shear measurements with increasing shear rates for a fixed time of 120 s for both (PLA/GNP)/EVA and PLA/(EVA/GNP) blends. Both PLA/EVA composition (50/50 wt. %) and GNP concentration (0.5 wt. %) are fixed. In Fig. 7(a), the growth of the shear stress is plotted as a function of shear strain. In both systems, the stress overshoot increases with the applied shear rate. It is notable that stress overshoots are visible even at the lowest shear rate of 0.01 s^{-1}; at extremely low shear rates, polymer chains are assumed to maintain their equilibrium entanglement density and do not produce stress overshoots during startup shear. The observed overshoot originates from the presence of GNPs, indicating the presence of a well-connected GNP particle network. This is also seen in previous studies of polymer/layered silicate [45] and polymer/nanoclay [46].

Our results show that (PLA/GNP)/EVA produces a higher stress overshoot as compared to PLA/(EVA/GNP) across the entire range of transient shear rates between 0.01 and 1 s^{-1} (higher shear rates are not studied due to edge failure and sample ejection from the test geometry). The interfacial GNPs produce a more robust three-dimensional percolating particle network to resist transient shear deformations, in addition to showing higher blend electrical conductivity and higher critical percolation coefficient as previously discussed. The difference in stress overshoots between two systems decreases with increasing shear rates. The peak of the stress overshoot occurs at similar shear strains (1.5–2 for the current system) regardless of shear rates, which is indicative of the filler particle network [47,48]. Lower shear rates require a longer time to reach the shear strain corresponding

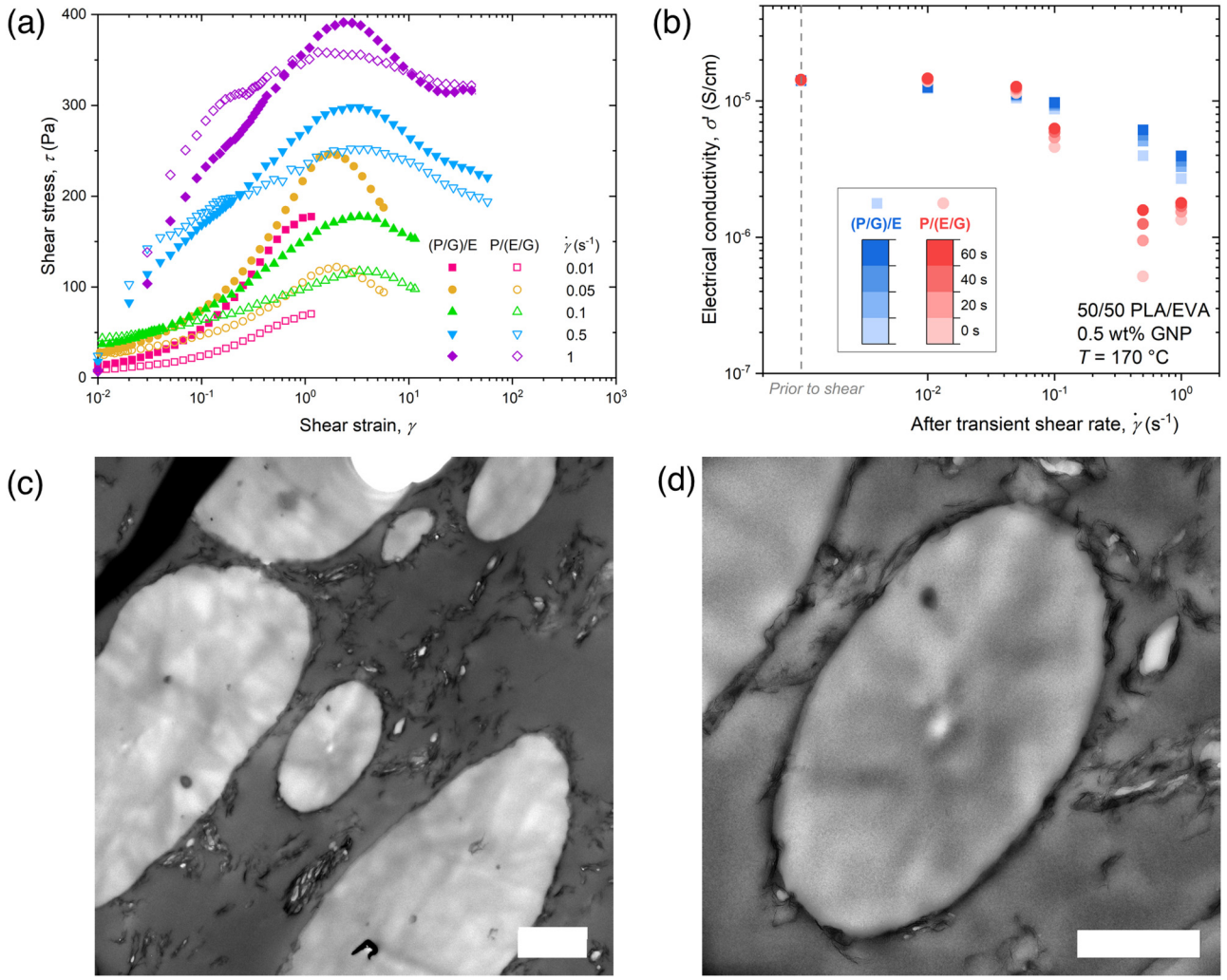

FIG. 7. (a) Startup shear experimental results for both (PLA/GNP)/EVA and PLA/(EVA/GNP) systems with 0.5 wt. % GNP for different shear rates, plotted as the growth of shear stress as a function of shear strain; (b) electrical conductivity of both (PLA/GNP)/EVA and PLA/(GNP/EVA) systems prior to or after each step of startup shear; (c) and (d) morphology of the (PLA/GNP)/EVA system immediately quenched after the 1.0 s^{-1} startup shear rate, at a final shear strain of 120. In (c), scale bar = 2 μm. The center portion of (c) is taken at a higher magnification shown in (d), with scale bar = 1 μm.

to the maximum shear stress. This is because low shear rate flows can exfoliate GNP agglomerates and help adjacent particles establish contact with each other, thereby improving the GNP network structure [49]. Higher shear rates require a shorter time to reach the maximum shear stress, during which structure build-up can occur. Therefore, at higher shear rates, the filler network becomes more deformed due to shear flow irrespective of GNP localization, and the stress growth profiles of (PLA/GNP)/EVA and PLA/(EVA/GNP) blends are more similar. In Fig. S9 in the supplementary material [60], we provide the transient viscosity as a function of time for startup shear. Like the stress growth profiles, at lower shear rates (0.01–0.1 s^{-1}), the transient shear viscosities of the (PLA/GNP)/EVA sample are significantly higher than those of the PLA/(EVA/GNP) sample at corresponding shear rates. At high shear rates (>0.5 s^{-1}), the transient shear viscosities between the two samples are comparable regardless of GNP localization.

Upon cessation of startup shear, we immediately perform dielectric measurements to characterize the state of the conductive GNP network and to determine whether the conductive filler network has been permanently disrupted by nonlinear shearing. In Fig. 7(b), we plot the evolution of the real part of the complex conductivity as a function of imposed shear rates for both (PLA/GNP)/EVA and PLA/(EVA/GNP) samples. Electrical conductivities of the samples are measured prior to the first transient shear step; after loading, samples are quiescently annealed at 170 °C for ∼1 h [49]. The initial electrical conductivities of the two sets of samples with different GNP localizations are nearly identical at $\sim 1.5 \times 10^{-5}$ S/cm. Given that low shear rates result in little change in electrical conductivity, the microstructure of the composite must be little disrupted. At high shear rates (≥0.1 s^{-1}), the electrical conductivity of both (PLA/GNP)/EVA and PLA/(EVA/GNP) samples is lowered by up to one order of magnitude. In response to high shear strains and strain rates, the GNP network breaks down and individual GNP sheets orient in the direction of the shear gradient [5,6,50,51].

However, the electrical conductivities of both sets of composites immediately start to improve within the first minute after cessation of each transient shear step [Fig. 7(b)]. Blends with interfacial GNPs better recover electrical conductivity

after shearing. Within 60 s of annealing, the electrical conductivity of (PLA/GNP)/EVA with 0.5 wt. % GNP concentration sheared at 1 s^{-1} recovers to ~30% of the initial conductivity prior to startup shear, whereas the conductivity of PLA/(EVA/GNP) with identical GNP concentration only recovers to ~13% of its initial value. Postprocessing annealing allows previously perturbed and aligned particle networks to recover via unbending of bent GNP sheets during earlier processing, attractive interactions between adjacent graphene sheets, and Brownian diffusion of individual GNP sheet [49,52]. Additionally, due to viscoelasticity of the polymer matrix, the stretched-out polymer phases will recoil, reducing interfacial area and bringing back the interfacial contacts between GNP sheets. Moreover, the reduction of surface area in recoiled polymers can also lead to leaching out of interfacial GNPs into the EVA phase, thereby providing additional contact points in the interphase connectivity of GNPs within EVA [Figs. 7(c) and 7(d)]. Thus, the electrical conductivity of the polymer/graphene composites continues to improve with increasing annealing time after shear. The (PLA/GNP)/EVA system exhibits faster recovery in electrical conductivity as compared to the PLA/(EVA/GNP) system, indicating that the interfacial GNP network is still largely intact. The interfacial GNP network preserves electrical conductivity more significantly than when GNPs localize in the EVA phase. In Fig. S10 in the supplementary material [60], (PLA/GNP)/EVA blends consistently exhibit higher electrical conductivity and faster recovery when compared to PLA/(EVA/GNP) blends following a range of startup shear rates (0.01–1.0 s^{-1}) and GNP concentrations (0.1–1.0 wt. %). Most notably, the (PLA/GNP)/EVA blends with 1.0 wt. % GNP show almost no loss of electrical conductivity up to a final shear strain of 120.

From TEM imaging of the (PLA/GNP)/EVA system quenched immediately after shearing at 1.0 s^{-1} reaching a final strain of 120, a large number of GNPs are seen to remain at the polymer blend interface, preserving the conductive filler network and electrical conductivity [Figs. 7(c) and 7(d)]. Further recovery in G' is also observed after shearing (Fig. S11 in the supplementary material [60]). These results suggest that moderately high shear rates during processing do not significantly change the localization of the interfacial GNP network. The reduction in electrical conductivity may also be attributed to the partial breakup of the cocontinuous blend morphology as well as encapsulation of GNP, as shown in lower magnification images such as Fig. 7(c) and Fig. S6 in the supplementary material [60]. Nonetheless, a large fraction of interfacial area is covered with GNPs, showing the robustness of interfacial GNP network.

3. Extensional rheometry

In addition to nonlinear shear deformations, we perform a series of extensional rheology measurements for both sets of ternary polymer composites and the PLA/EVA neat blend to study the effect of extensional deformation on the interfacial GNP network formed by the two-step compounding sequence. The extensional stress is plotted as a function of the Hencky strain in Fig. 8(a). The extensional viscosities of the polymer/GNP composites are higher than that of the neat polymer blend due to the additional elasticity imparted by the filler particles. Similar to transient shear, at a low extensional rate of 0.01 s^{-1}, the extensional stress of the (PLA/GNP)/EVA blend is about twice that of the PLA/(EVA/GNP) blend for the duration of the experiments. Additionally, the (PLA/GNP)/EVA blend achieve a much higher strain at break, reaching a final Hencky strain of ~1.0 while both the PLA/(EVA/GNP) and the neat PLA/EVA blend have a similar strain at breaks at a Hencky strain of ~0.2. These results further show that the highly connected interfacial GNP network present in the (PLA/GNP)/EVA blends resists extensional deformation at low Hencky strains, showing enhanced melt strength. On the other hand, at a high extensional rate of 0.1 s^{-1}, there is no pronounced difference between the extensional stresses or strain at breaks between (PLA/GNP)/EVA and PLA/(EVA/GNP).

While dielectric measurements are not available for extensional rheology, TEM imaging provides insights into the blend morphology as well as the state of GNP networks following extensional deformation. Immediately upon the end of the extensional rheology measurements, samples are quickly removed from the test fixture and quenched in liquid nitrogen to freeze the morphology. Then, we embed parts of the remaining sample close to the point of breakage into a liquid epoxy for TEM sample preparation. Each specimen is oriented parallel with the direction of extensional deformation, and thin sections are obtained by cryo-microtomy. Figures 8(b)–8(d) show the resulting morphologies of the (PLA/GNP)/EVA, PLA/(EVA/GNP), and PLA/EVA neat blends, respectively; lower magnification images are provided in Fig. S12 in the supplementary material [60]. Despite reaching a final Hencky strain of ~1, Fig. 8(b) shows that in (PLA/GNP)/EVA blends a large number of GNP sheets remain on the PLA/EVA interface after extensional deformation. At this Hencky strain, the total interfacial area will have increased by a factor of e (~2.7), which requires GNPs to spread out and cover the newly generated interface. TEM imaging shows that the interfacial GNP sheets form good contacts with adjacent sheets after extensional deformation. In several local regions, interfacial GNP forms particle-jammed, irregularly shaped droplets. This is in contrast with Figs. 8(c) and 8(d): when GNPs are absent from the PLA/EVA interface, the blend assumes a droplet-matrix morphology upon extensional deformation with the lighter PLA phase appearing as rounded spherical droplets.

Mei *et al.* studied hydrophobic silica particles that thermodynamically localize at the interface of a poly(isobutylene)/poly(dimethylsiloxane) (PIB/PDMS) suspension [53]. They proposed a mechanism that produces irregularly shaped, particle-covered droplets from shear deformations. When the capillary number exceeds a critical value for which either shear or extensional deformation overcomes the interfacial tension, large droplets in polymer blends break up into two smaller droplets due to capillary instability. However, when particles cover the fluid interface, localized interfacial roughness is preserved by the elastic particle network. The numerous bends and protrusions arising from fluid deformation will eventually evolve into buckled interfaces and irregularly shaped droplets

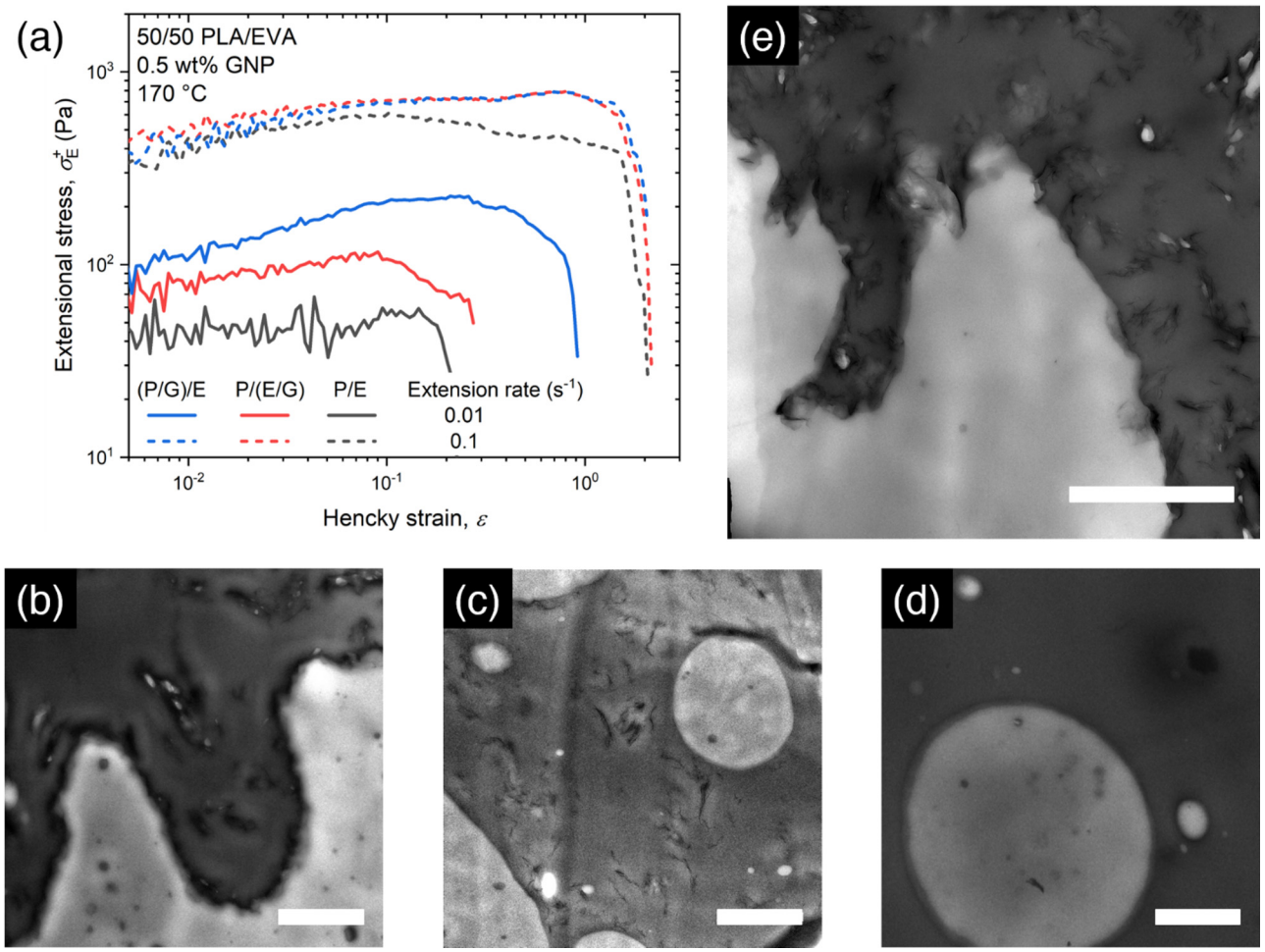

FIG. 8. (a) Extensional stress profiles as a function of Hencky strain for constant extensional rates for (PLA/GNP)/EVA, PLA/(GNP/EVA), and unfilled PLA/EVA systems. (b)–(d) the TEM morphology of the three systems taken at strain to break (~1) after an extension rate of 0.01 s^{-1}, respectively. (e) The TEM morphology of the (PLA/GNP)/EVA system taken at strain of break (~1) after an extension rate of 0.1 s^{-1}. In both (b) and (e), GNPs are seen to fully cover the PLA/EVA interface. Scale bar = 2 μm for all images.

stabilized by interfacial particles [8,54–58]. The interfacial GNP network is stable with stronger extensional flow. While the final extensional stresses at break (Hencky strain ~1) are similar for both (PLA/GNP)/EVA and PLA/(EVA/GNP) under the higher extensional rate of 0.1 s^{-1}, TEM images [Fig. 8(e)] show that GNP network remains at the interface and produces irregularly shaped droplets. As twin-screw microcompounding imparts strong extensional mixing forces, the fact that electrical conductivities of (PLA/GNP)/EVA remain high after 10 min of compounding (Fig. 3) indicate that interfacial GNP network will remain present at even higher Hencky strains.

In summary, our kinetic trapping method to localize GNPs at the PLA/EVA interface produces robust interfacial networks of GNP showing high stability under nonlinear shear or extensional flows. Interfacial GNPs preserve the nonequilibrium morphology by forming adjacent particle-to-particle contacts, suppressing domain coarsening, and maintaining high levels of electrical conductivity [8]. We can further correlate results from rheological measurement with the melt compounding time studies shown in Fig. 3. The electrical conductivity of the (PLA/GNP)/EVA blend begins to show decrease only when compouding exceeds 10 min. Therefore, assuming the microcompounder operating at 100 rpm has an effective shear rate of 270 s^{-1} [8], the minimum shear strain required to remove trapped GNPs at the interface into the EVA phase is $\sim 1.6 \times 10^5$ strain units, which is significantly higher than the total shear strain of ~120 or a total Hencky strain of ~2 imparted in our rheological measurements. We anticipate that the GNP localization will remain at the interface under typical processing times, yielding highly electrically conductive blends. Moreover, the conductivity of the interfacial GNP network can improve via postprocessing annealing. While extensional deformation may also remove some GNPs from the interface into the EVA phase, the recoil of polymer chains after extensional deformation may also impart additional intra-phase connectivity of GNPs in the EVA phase [Figs. 8(b) and 8(e) and Figs. S12(a) and S12(b) in the supplementary material [60]]. Similar to post-startup shear experiments, post-processing annealing can further restore the electrical conductivity of these composites after extensional deformations.

IV. CONCLUSIONS

In this work, we create a cocontinuous polymer composite where GNPs are interfacially localized at the PLA/EVA

interface by kinetic trapping: GNPs are initially mixed with PLA, the thermodynamically unfavored component, and then melt compounded with EVA. The two-step compounding sequence is determined based on a wetting coefficient analysis: GNPs prefer EVA over PLA with the wetting coefficient $\omega > 1$. TEM and SEM results support the wetting coefficient analysis and confirm the interfacial localization of GNPs. Small amplitude shear and dielectric rheology both show GNPs form a percolated network at the interface of cocontinuous polymer blends, enhancing both the elastic modulus and electrical conductivity. Controlling the time of the second compounding step is essential to promote effective GNP migration from the PLA phase to the EVA phase. In the current system, to achieve effective kinetic trapping of GNPs at the interface, the optimal time of the second mixing step has a wide window of 2–10 min, based on improvement in the electrical conductivity. While GNPs leave PLA quickly during initial compounding, they are trapped for a long time at the interface. After long mixing, they eventually move to the EVA phase. Setting 2 min as the duration of the second mixing step, we are able to produce highly conductive (PLA/GNP)/EVA composites with an ultralow percolation threshold of 0.048 wt. %, one of the lowest values reported for GNPs in current literature (Table I).

The fact that high conductivity is maintained during 2–10 min melt compounding is strong evidence for robustness of the interfacial GNP network. Its strength is also verified via transient shear and extensional rheology. Blends with interfacially localized GNP networks are more resistant to nonlinear shear deformation, showing higher shear stress and increased transient shear viscosity. While startup shear up to $1.0\,s^{-1}$ could disrupt the GNP network by temporarily aligning nearby fillers and therefore reducing electrical conductivity, upon cessation of shear flow the system quickly recovers its electrical conductivity during annealing. TEM imaging shows a large number of GNPs preserve their interfacial localization in (PLA/GNP)/EVA, leading to faster conductivity recovery. Similarly, interfacial GNPs are effective at resisting extensional flow, resulting in enhanced melt extensional viscosity and strain at break. TEM imaging after extensional deformation further shows that the elastic particle network formed at the PLA/EVA interface produces irregularly shaped interfaces, which indicates GNP filler coverage.

In combination with our previous studies [9,10], we have demonstrated kinetic trapping as an effective general strategy of driving GNPs to the interface for different cocontinuous polymer blends. With proper control of compounding sequence and time, we successfully reduce the percolation threshold of GNPs in PLA/EVA blends to 0.048 wt. %. Our polymer/GNP composites with 0.5 wt. % filler concentration had an electrical conductivity of $\sim 10^{-5}$ S/cm when measured at 170 °C. The robust interfacial particle networks formed by kinetic trapping resist significant nonlinear shear and extensional deformations and remain electrically conductive. Further annealing after nonlinear deformation causes the interfacial particle network to undergo structural and electrical conductivity recovery. Therefore, our study illustrates advantageous features for the formulation of polymer/graphene composites for practical applications in electrostatic discharge protection [59].

ACKNOWLEDGMENTS

The authors thank Dr. Sam Dahman of RTP Corporation for helpful discussions. We gratefully acknowledge funding from the National Science Foundation (NSF) (No. CMMI-1661666), University of Minnesota Industrial Partnership for Research in Interfacial Materials & Engineering (IPRIME), and the University of Minnesota Rheology Short Course. Parts of this work were carried out in the Characterization Facility, University of Minnesota, a member of the NSF-funded Materials Research Facilities Network (www.mrfn.org) via the MRSEC program.

REFERENCES

[1] Stankovich, S., D. A. Dikin, G. H. B. Dommett, K. M. Kohlhaas, E. J. Zimney, E. A. Stach, R. D. Piner, S. B. T. Nguyen, and R. S. Ruoff, "Graphene-based composite materials," Nature **442**, 282–286 (2006).

[2] Mao, C., Y. Zhu, and W. Jiang, "Design of electrical conductive composites: Tuning the morphology to improve the electrical properties of graphene filled immiscible polymer blends," ACS Appl. Mater. Interfaces **4**, 5281–5286 (2012).

[3] Qi, X. Y., D. Yan, Z. Jiang, Y. K. Cao, Z. Z. Yu, F. Yavari, and N. Koratkar, "Enhanced electrical conductivity in polystyrene nanocomposites at ultra-low graphene content," ACS Appl. Mater. Interfaces **3**, 3130–3133 (2011).

[4] Liebscher, M., M. O. Blais, P. Pötschke, and G. Heinrich, "A morphological study on the dispersion and selective localization behavior of graphene nanoplatelets in immiscible polymer blends of PC and SAN," Polymer **54**, 5875–5882 (2013).

[5] Kou, Y., X. Cheng, and C. W. Macosko, "Polymer/graphene composites via spinodal decomposition of miscible polymer blends," Macromolecules **52**, 7625–7637 (2019).

[6] Vleminckx, G., S. Bose, J. Leys, J. Vermant, M. Wübbenhorst, A. A. Abdala, C. Macosko, and P. Moldenaers, "Effect of thermally reduced graphene sheets on the phase behavior, morphology, and electrical conductivity in poly[(α-methyl styrene)-co-(acrylonitrile)/poly(methyl-methacrylate) blends," ACS Appl. Mater. Interfaces **3**, 3172–3180 (2011).

[7] Imperiali, L., K. H. Liao, C. Clasen, J. Fransaer, C. W. Macosko, and J. Vermant, "Interfacial rheology and structure of tiled graphene oxide sheets," Langmuir **28**, 7990–8000 (2012).

[8] Bai, L., S. He, J. W. Fruehwirth, A. Stein, C. W. Macosko, and X. Cheng, "Localizing graphene at the interface of cocontinuous polymer blends: Morphology, rheology, and conductivity of cocontinuous conductive polymer composites," J. Rheol. **61**, 575–587 (2017).

[9] Bai, L., R. Sharma, X. Cheng, and C. W. Macosko, "Kinetic control of graphene localization in co-continuous polymer blends via melt compounding," Langmuir **34**, 1073–1083 (2018).

[10] Mun, S. C., M. J. Kim, M. Cobos, L. Gu, and C. W. Macosko, "Strategies for interfacial localization of graphene/polyethylene-based cocontinuous blends for electrical percolation," AIChE J. **65**, e16579 (2019).

[11] Yoshida, S., and M. Trifkovic, "Unraveling the effect of 3D particle localization on coarsening dynamics and rheological properties in cocontinuous polymer blend nanocomposites," Macromolecules **52**, 7678–7687 (2019).

[12] Gubbels, F., R. Jérôme, P. Teyssié, E. Vanlathem, R. Deltour, A. Calderone, V. Parenté, and J. L. Brédas, "Selective localization of carbon black in immiscible polymer blends: A useful tool To design electrical conductive composites," Macromolecules **27**, 1972–1974 (1994).

[13] Gubbels, F., S. Blacher, E. Vanlathem, R. Jérôme, R. Deltour, F. Brouers, and P. Teyssié, "Design of electrical conductive composites: Key role of the morphology on the electrical properties of carbon black filled polymer blends," Macromolecules **28**, 1559–1566 (1995).

[14] Gubbels, F., R. Jerome, E. Vanlathem, R. Deltour, S. Blacher, and F. Brouers, "Kinetic and thermodynamic control of the selective localization of carbon black at the interface of immiscible polymer blends," Chem. Mater. **10**, 1227–1235 (1998).

[15] Zaikin, A. E., R. R. Karimov, and V. P. Arkhireev, "A study of the redistribution conditions of carbon black particles from the bulk to the interface in heterogeneous polymer blends," Colloid J. **63**, 53–59 (2001).

[16] Katada, A., Y. F. Buys, Y. Tominaga, S. Asai, and M. Sumita, "Relationship between electrical resistivity and particle dispersion state for carbon black filled poly (ethylene-co-vinyl acetate)/poly (L-lactic acid) blend," Colloid Polym. Sci. **284**, 134–141 (2005).

[17] Briggs, N. M., J. S. Weston, B. Li, D. Venkataramani, C. P. Aichele, J. H. Harwell, and S. P. Crossley, "Multiwalled carbon nanotubes at the interface of Pickering emulsions," Langmuir **31**, 13077–13084 (2015).

[18] Wu, D., Y. Zhang, M. Zhang, and W. Yu, "Selective localization of multiwalled nanotubes in poly(ϵ-caprolactone)/polylactide blend," Biomacromolecules **10**, 417–424 (2009).

[19] Chen, J., Y. Y. Shi, J. H. Yang, N. Zhang, T. Huang, C. Chen, Y. Wang, and Z. W. Zhou, "A simple strategy to achieve very low percolation threshold via the selective distribution of carbon nanotubes at the interface of polymer blends," J. Mater. Chem. **22**, 22398–22404 (2012).

[20] Baudouin, A. C., J. Devaux, and C. Bailly, "Localization of carbon nanotubes at the interface in blends of polyamide and ethylene-acrylate copolymer," Polymer **51**, 1341–1354 (2010).

[21] Bose, S., C. Özdilek, J. Leys, J. W. Seo, M. Wübbenhorst, J. Vermant, and P. Moldenaers, "Phase separation as a tool to control dispersion of multiwall carbon nanotubes in polymeric blends," ACS Appl. Mater. Interfaces **2**, 800–807 (2010).

[22] Shi, Y., J. Yang, T. Huang, N. Zhang, C. Chen, and Y. Wang, "Selective localization of carbon nanotubes at the interface of poly(L-lactide)/ethylene-co-vinyl acetate resulting in lowered electrical resistivity," Compos. Part B Eng. **55**, 463–469 (2013).

[23] Göldel, A., A. Marmur, G. R. Kasaliwal, P. Pötschke, and G. Heinrich, "Shape-dependent localization of carbon nanotubes and carbon black in an immiscible polymer blend during melt mixing," Macromolecules **44**, 6094–6102 (2011).

[24] Huang, J., Y. Zhu, L. Xu, J. Chen, W. Jiang, and X. Nie, "Massive enhancement in the thermal conductivity of polymer composites by trapping graphene at the interface of a polymer blend," Compos. Sci. Technol. **129**, 160–165 (2016).

[25] Shen, Y., T. T. Zhang, J. H. Yang, N. Zhang, T. Huang, and Y. Wang, "Selective localization of reduced graphene oxides at the interface of PLA/EVA blend and its resultant electrical resistivity," Polym. Compos. **38**, 1982–1991 (2017).

[26] Tu, C., K. Nagata, and S. Yan, "Influence of melt-mixing processing sequence on electrical conductivity of polyethylene/polypropylene blends filled with graphene," Polym. Bull. **74**, 1237–1252 (2017).

[27] Helal, E., R. S. Kurusu, N. Moghimian, G. Gutierrez, E. David, and N. R. Demarquette, "Correlation between morphology, rheological behavior, and electrical behavior of conductive cocontinuous LLDPE/EVA blends containing commercial graphene nanoplatelets," J. Rheol. **63**, 961–976 (2019).

[28] Hadaeghnia, M., S. Ahmadi, I. Ghasemi, and P. M. Wood-Adams, "Manipulating the morphology of PA6/POE blends using graphene to achieve balanced electrical and mechanical properties," Compos. Sci. Technol. **200**, 108412 (2020).

[29] Electrostatic Discharge Association, *ESD Association Standard for the Protection of Electrostatic Discharge Susceptible Items – Packaging Materials for ESD Sensitive Items (ANSI/ESD S541-2008)* (Electrostatic Discharge Association, New York, 2008).

[30] Ni, Z. H., H. M. Wang, J. Kasim, H. M. Fan, T. Yu, Y. H. Wu, Y. P. Feng, and Z. X. Shen, "Graphene thickness determination using reflection and contrast spectroscopy," Nano Lett. **7**, 2758–2763 (2007).

[31] Alig, I., P. Pötschke, D. Lellinger, T. Skipa, S. Pegel, G. R. Kasaliwal, and T. Villmow, "Establishment, morphology and properties of carbon nanotube networks in polymer melts," Polymer **53**, 4–28 (2012).

[32] Taguet, A., P. Cassagnau, and J. M. Lopez-Cuesta, "Structuration, selective dispersion and compatibilizing effect of (nano)fillers in polymer blends," Prog. Polym. Sci. **39**, 1526–1563 (2014).

[33] Dai, J., G. Wang, L. Ma, and C. Wu, "Study on the surface energies and dispersibility of graphene oxide and its derivatives," J. Mater. Sci. **50**, 3895–3907 (2015).

[34] Wang, S., Y. Zhang, N. Abidi, and L. Cabrales, "Wettability and surface free energy of graphene films," Langmuir **25**, 11078–11081 (2009).

[35] Leonard, D. J., L. T. Pick, D. F. Farrar, G. R. Dickson, J. F. Orr, and F. J. Buchanan, "The modification of PLA and PLGA using electron-beam radiation," J. Biomed. Mater. Res. Part A **89A**, 567–574 (2009).

[36] Dutta, J., T. Chatterjee, G. Dhara, and K. Naskar, "Exploring the influence of electron beam irradiation on the morphology, physico-mechanical, thermal behaviour and performance properties of EVA and TPU blends," RSC Adv. **5**, 41563–41575 (2015).

[37] Marić, M., and C. W. Macosko, "Improving polymer blend dispersion in mini-mixers," Polym. Eng. Sci. **41**, 118–130 (2001).

[38] Kim, H., and C. W. Macosko, "Processing-property relationships of polycarbonate/graphene composites," Polymer **50**, 3797–3809 (2009).

[39] Baudouin, A.-C., C. Bailly, and J. Devaux, "Interface localization of carbon nanotubes in blends of two copolymers," Polym. Degrad. Stab. **95**, 389–398 (2010).

[40] Jalali Dil, E., and B. D. Favis, "Localization of micro- and nano-silica particles in heterophase poly(lactic acid)/poly(butylene adipate-co-terephthalate) blends," Polymer **76**, 295–306 (2015).

[41] Blake, T. D., and J. De Coninck, "The influence of solid-liquid interactions on dynamic wetting," Adv. Colloid Interface Sci. **96**, 21–36 (2002).

[42] Blake, T. D., "The physics of moving wetting lines," J. Colloid Interface Sci. **299**, 1–13 (2006).

[43] Mohammadi, M., M.-C. Heuzey, P. J. Carreau, and A. Taguet, "Morphological and rheological properties of PLA, PBAT, and PLA/PBAT blend nanocomposites containing CNCs," Nanomaterials **11**, 857 (2021).

[44] Dubson, M. A., and J. C. Garland, "Measurement of the conductivity exponent in two-dimensional percolating networks: Square lattice versus random-void continuum," Phys. Rev. B **32**, 7621–7623 (1985).

[45] Gupta, R. K., V. Pasanovic-Zujo, and S. N. Bhattacharya, "Shear and extensional rheology of EVA/layered silicate-nanocomposites," J. Non-Newtonian Fluid Mech. **128**, 116–125 (2005).

[46] Eslami, H., M. Grmela, and M. Bousmina, "Linear and nonlinear rheology of polymer/layered silicate nanocomposites," J. Rheol. **54**, 539–562 (2010).

[47] Solomon, M. J., A. S. Almusallam, K. F. Seefeldt, A. Somwangthanaroj, and P. Varadan, "Rheology of polypropylene/clay hybrid materials," Macromolecules **34**, 1864–1872 (2001).

[48] Letwimolnun, W., B. Vergnes, G. Ausias, and P. J. Carreau, "Stress overshoots of organoclay nanocomposites in transient shear flow," J. Non-Newtonian Fluid Mech. **141**, 167–179 (2007).

[49] Boothroyd, S. C., D. W. Johnson, M. P. Weir, C. D. Reynolds, J. M. Hart, A. J. Smith, N. Clarke, R. L. Thompson, and K. S. Coleman, "Controlled structure evolution of graphene networks in polymer composites," Chem. Mater. **30**, 1524–1531 (2018).

[50] Kim, H., and C. W. Macosko, "Morphology and properties of polyester/exfoliated graphite nanocomposites," Macromolecules **41**, 3317–3327 (2008).

[51] Vermant, J., S. Ceccia, M. K. Dolgovskij, P. L. Maffettone, and C. W. Macosko, "Quantifying dispersion of layered nanocomposites via melt rheology," J. Rheol. **51**, 429–450 (2007).

[52] Happel, J., and H. Brenner, *Low Reynolds Number Hydrodynamics* (Springer, Dordrecht, 1973).

[53] Mei, Y., Li, G., Moldenaers, P., and R. Cardinaels, "Dynamics of particle-covered droplets in shear flow: unusual breakup and deformation hysteresis," Soft Matter **12**, 9407–9412 (2016).

[54] Tavacoli, J. W., J. H. J. Thijssen, A. B. Schofield, and P. S. Clegg, "Novel, robust, and versatile Bijels of nitromethane, ethanediol, and colloidal silica: Capsules, sub-ten-micrometer domains, and mechanical properties," Adv. Funct. Mater. **21**, 2020–2027 (2011).

[55] Witt, J. A., D. R. Mumm, and A. Mohraz, "Bijel reinforcement by droplet bridging: A route to bicontinuous materials with large domains," Soft Matter **9**, 6773–6780 (2013).

[56] Vandebril, S., J. Vermant, and P. Moldenaers, "Efficiently suppressing coalescence in polymer blends using nanoparticles: Role of interfacial rheology," Soft Matter **6**, 3353–3362 (2010).

[57] Huang, S., L. Bai, M. Trifkovic, X. Cheng, and C. W. Macosko, "Controlling the morphology of immiscible cocontinuous polymer blends via silica nanoparticles jammed at the interface," Macromolecules **49**, 3911–3918 (2016).

[58] Bai, L., J. W. Fruehwirth, X. Cheng, and C. W. Macosko, "Dynamics and rheology of nonpolar Bijels," Soft Matter **11**, 5282–5293 (2015).

[59] Hu, K., D. D. Kulkarni, I. Choi, and V. V. Tsukruk, "Graphene-polymer nanocomposites for structural and functional applications," Prog. Polym. Sci. **39**, 1934–1972 (2014).

[60] See supplementary material at https://www.scitation.org/doi/suppl/10.1122/8.0000294 for additional characterization of neat polymers, discussion on specific energy of melt compounding, surface energies, supplementary dielectric rheology data, and TEM images of the blends.